Original Article

Institution of MECHANICAL ENGINEERS

Journal of AEROSPACE ENGINEERING

Proc IMechE Part G:
J Aerospace Engineering
0(0) 1–12

DOI: 10.1177/0954410017717285
journals.sagepub.com/home/pig

SAGE

Obtaining minimum-drag shapes through surrogate-based global optimization: An application to the aerodynamic shape design of the landing gear master cylinder

Esther Andrés-Pérez[1,2], Daniel González-Juárez[3], Mario J Martin-Burgos[3], Leopoldo Carro-Calvo[4] and Sancho Salcedo-Sanz[4]

Abstract

Nowadays, one of the priorities of the European Commission is to reduce the environmental impact of aviation through the advanced design of novel aircraft configurations. This is of utmost importance in order to decrease the environmental footprint of aviation and to reduce fuel consumption and make airlines more profitable. This implies that new methods and tools for aerodynamic shape optimization will have to be developed, allowing aircraft configurations that cannot be obtained with traditional strategies. This paper focuses on the application of enhanced methods in aerodynamic shape design optimization to enable advanced aircraft configurations. In particular, this work aims to demonstrate the feasibility of the proposed strategy to reach optimal configurations that are far away from its baseline geometry. For this purpose, evolutionary algorithms are combined with support vector machines and applied to the optimization of a baseline geometry for different flow conditions. In particular, the selected application is based on the shape optimization problem of the landing gear master cylinder. Results pointed out the feasibility of the mentioned strategy to enable novel configurations within an aerodynamic shape optimization process.

Keywords

Aerodynamic shape optimization, evolutionary algorithms, support vector machines, computational fluid dynamics

Date received: 14 March 2016; accepted: 1 June 2017

Introduction

Currently, there is a strong need for efficient aerodynamic shape optimization tools for the industrial aircraft design that enables the emergence of the new aircraft generation, able to satisfy the objectives stated in the ACARE 2020[1] and 2050[2] flight paths. Nowadays, traditional aircraft shapes are already optimized, and small and local changes in these configurations are no longer providing noticeable improvements in the performance. Therefore, it is necessary to target completely innovative shapes through large deformations and global explorations of the design space, in order to move forward to the aircraft shapes that will be demanded by the aeronautical industry in the following decades. Considering this, aerodynamic shape design and optimization problems based on evolutionary programming and surrogate models (also called surrogate-based optimization or SBO) have recently found widespread use in aeronautics, due to the potential to reach optimal configurations that are far away from their baseline geometries, and therefore, their ability to enable non-conventional aircraft configurations. In addition, their increasing applicability in aerodynamic shape optimization problems is also due to the promising potential of these methods to speed up the whole design process by the use of a "low-cost" objective function evaluation to reduce the

[1]Ingeniería de Sistemas para la Defensa de España (ISDEFE), Fluid Dynamics Branch, Spanish National Institute for Aerospace Technology (INTA), Madrid, Spain
[2]Department of Physics, Automatics, Electronics and Informatics, Technical University of Madrid (UPM), Madrid, Spain
[3]Department of Aerodynamics and Propulsion, Fluid Dynamics Branch, National Institute for Aerospace Technology (INTA), Madrid, Spain
[4]Department of Signal Theory and Communications, University of Alcalá (UAH), Alcalá de Henares, Spain

Corresponding author:
Esther Andrés-Pérez, INTA/ISDEFE, Ctra. de Ajalvir, km. 4.5, Torrejón de Ardoz, Madrid 28850, Spain.
Email: eandres@isdefe.es

required number of expensive computational fluid dynamics (CFD) simulations.

However, the application of these SBO methods for industrial configurations faces several challenges. The most crucial challenges nowadays is the so-called ''curse of dimensionality'', the ability of surrogates when handling a high number of design parameters, efficient constraints handling, adequate exploration and exploitation of the design space, and last but not least, how to deal with grid deformations in case of large displacements, which is always the case when trying to achieve novel configurations from the traditional ones.

This work focuses on the application of enhanced methods in aerodynamic shape design optimization to enable novel aircraft configurations. In particular, it aims to demonstrate the feasibility of a combined approach, based on evolutionary algorithms (EAs) and support vector machines (SVMs), to reach optimal configurations that are far away from the baseline geometry. In order to validate this, the optimization approach is applied to the selected baseline geometry, a landing gear master cylinder, resulting in optimal configurations for each of the defined flow conditions. This very simple test case (clean cylinder) has been selected for several reasons: it will allow validation of the potential of the proposed approach to reach non-conventional configurations (those which are far from the initial one), and in addition, it is of interest for a European aircraft manufacturing industry, which is looking for flow optimization in this region. However, in order to further exploit the results in industry, more complex geometries and constraints, including also structural aspects, should have to be taken into consideration.

The paper is structured as follows: the section following provides a literature review on surrogate-based aerodynamic shape optimization methods in aeronautics. Then, the approach to be applied is detailed, including the parameterization strategy, the EA and support vector machines for regression (SVMR) approach, giving details on the EA and SVMR algorithms. Then, the experimental part of the paper is explained, where different results on the optimized geometries are outlined. Finally, the last section draws some conclusions and suggests future activities.

Literature review on aerodynamic optimization for non-conventional shapes

In general, optimization methods can be roughly classified as deterministic, i.e. gradient-based methods and stochastic. The use of the adjoint approach[3–10] allows for the calculation of gradients very efficiently, since the number of required executions is essentially independent from the number of design parameters. However, gradient-based methods require a continuous evaluation function and perform poorly in a noisy design space, while they also strongly depend on the baseline configuration, as frequently, they get trapped into local minima. On the other hand, non-deterministic methods, such as EAs, are able to cope with complex, constrained, noisy objective functions, as a black box, without assumptions of continuity or linearity[11] of the objective function. However, these methods need a lot of evaluations to get the optimum solution, even when considering only a small number of design variables. For this reason, surrogate models are used as fast evaluators that replace time-consuming CFD simulations at a cost of precision. Depending on the training method, surrogate models are classified as off-line[12] and on-line learning,[13] in which a selected number of candidates are sent to the CFD solver in order to improve the accuracy of the model.

Surrogate methods, based on artificial neural networks (ANNs), have been successfully employed as a predictor of aerodynamic coefficients in the shape optimization of simple configurations.[14–16] In addition, SVMs have been also applied for prediction in many areas, such as finances or energy.[17–21]

With respect to SBO applied to aerodynamic shape design of aeronautical configurations, there have been several approaches[22–28] in the last years trying to employ different surrogates (for instance, Kriging, Proper Orthogonal Decomposition, ANNs, etc.) and geometry parameterization techniques (PARSEC, Class Shape Transformation method, etc.).

To conclude, the authors have also published recent research on this topic[29–31] applying an SBO method to the aerodynamic shape optimization of an RAE2822 two-dimensional airfoil and a Drag prediction workshop (DPW) three-dimensional wing. However, the work presented here is, to the authors' knowledge, the first time in the literature that an SBO strategy is applied to a simple ''dummy'' baseline geometry in order to validate its ability to globally explore the design space and provide optimal geometries. Moreover, the application of this research to industry is also provided by the test case selection, a landing gear master cylinder, which is optimized for certain take-off and landing flow conditions.

SBO strategy

Geometry parameterization

The cylinder grid is deformed through a volumetric B-spline, as shown in Figure 1. The design variables are the control points located on the upper and lower side, which can freely move in any direction, while the control points located in the middle are kept fixed during optimization. In this method, the original geometry is deformed by the movement of control points in a similar way than the free form deformation (FFD) technique,[32] but in contrast to FFD, deformations of the upper side and lower side can

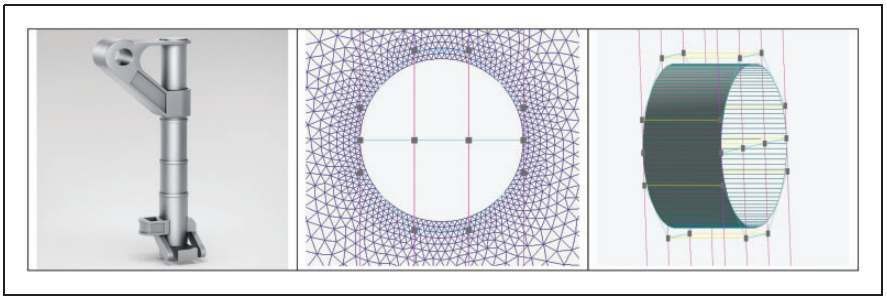

Figure 1. Landing gear master cylinder (left, source: Walter tools, http://www.walter-tools.com). Parameterization of the cylinder: 2D (center) and 3D (right) views.

be considered independent of each other, which provides more flexibility.

The computational surface grid vertices are mapped into the NURBS (non-uniform rational B-splines) space through the parametric coordinates, which are previously calculated using an appropriate inversion point algorithm.[4,33] These parametric coordinates are invariant throughout the optimization, allowing to recalculate the spatial coordinates at any time of the process. A second mapping is performed on the cylinder geometry, by means of a discrete uniform rasterization, in order to accurately calculate the volume throughout the optimization. This geometry mapping is done in parallel, independently of the computational grid and it is used for handling the volume constraint within the optimization process.

The cylinder is modeled as an extruded geometry and the control points on both sides are moved symmetrically; so in total, eight design control points are considered.

The mathematical definition that governs the geometry deformation is

$$X = \sum_i \sum_j B_i(u) B_j(v) \cdot C_{ij} \tag{1}$$

where X are the Cartesian coordinates, C_{ij} are the control points, B are the basis functions, and u and v are the parametric coordinates. In this problem, the basis functions in the chord direction correspond to second-order Bernstein polynomials to the interval [0,1]

$$B_0 = (1-u)^2, \quad B_1 = 2u(1-u), \quad B_2 = u^2 \tag{2}$$

while the vertical direction is represented by a linear deformation, making the upper side and the lower side independent. Bernstein polynomials provide useful properties for aerodynamic design: basis functions are symmetric $B_i(t) = B_{n-i}(1-t)$. The sum of the basis function is always 1, so normalization is not required. Each basis function has one single unique maximum, which ensures the convergence when calculating the parametric coordinates. Basis functions are always positive; negative basis function causes oscillations of the curvature, which is undesired in aerodynamic design. For optimization problems, the maximum and minimum values are always bounded; hence, the deformed geometry will always remain contained inside the control box.

The volume of the deformed geometry is calculated using the trapezoidal rule as

$$\begin{aligned} V &= \int_{upperside} X(u,v)\mathrm{d}x - \int_{lowerside} X(u,v)\mathrm{d}x \\ &\approx \sum_{lowerside} \frac{X_{i+1} + X}{2(N-1)} \approx \sum_{upperside} \frac{X_{i+1} + X}{2(N-1)} \end{aligned} \tag{3}$$

where X_{i+1} and X_i are consecutive points and N is the number of points selected.

Selected SBO strategy

In this paper, the "intelligent estimation search with sequential learning (IES-SL)" approach[31] is used. The IES-SL allows to perform a broad exploration of the design space, by the use of an adaptive sampling based on the objective function.[34] Therefore, this method specially explores those regions of the design space where the optima are located. This approach is illustrated in Figure 2.

One of the main characteristics of the approach is the use of the surrogate model (SVMs in this paper) to estimate the location of the optimum. The following steps are performed:

1. First, an initial surrogate is built by using a reduced database of high fidelity samples (in this work, this initial database is composed of four random geometries plus the baseline geometry).
2. The search is then applied over the surrogate, which means that in each optimization iteration, a new estimated optimum is returned (which is also called "an intelligent guess"[35]).
3. Then, the estimated optimum is computed using the high fidelity CFD solver.
4. This new high fidelity value is incorporated to the database, and the surrogate model is rebuilt.

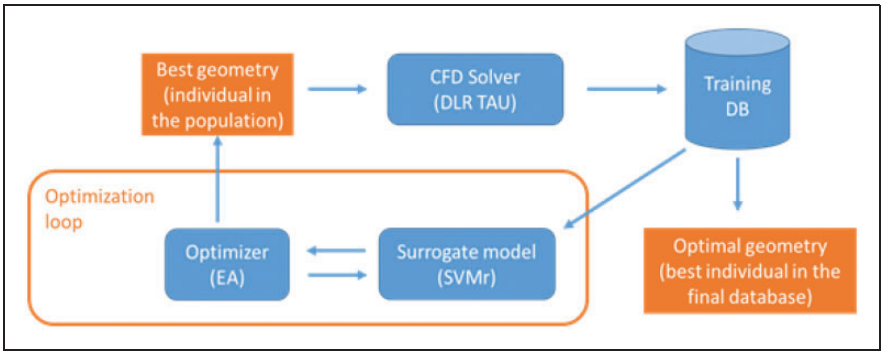

Figure 2. Flowchart of the SBO process.
CFD: computational fluid dynamics; DB: database; EA: evolutionary algorithm; SVM: support vector machine. TAU is the computational fluid dynamics code used (property of the German Aerospace Center, DLR).

5. A new optimization iteration starts on the new surrogate and provides a new estimated optimum. Then, the algorithm continues in step 3.

In this way, the sampling is directly focusing on the objective function. The optimization algorithm finishes when a certain number of iterations is reached, and then, the optimum shape is the element with the best parameters in the database.

In this paper, the specific details on the EA, SVMs and objective function calculation with the DLR TAU solver have not been included, but the reader can consult the literature[29–31,36,37] for the implementation details.

Within the proposed methodology, the EA ensures that the global optimum is reached while the CFD validation and surrogate reconstruction ensures the approach accuracy.

Although, in the literature, there are other approaches for the enhancement of the surrogate model accuracy (i.e. see state-of-the-art methods in earlier studies[38–40]), the presented approach is based on SVMs for regression as the surrogate model technique, and the main novelty is its application for aerodynamic shape optimization. In fact, this is, to the authors' knowledge, the first time that an SBO strategy (based on SVMs) is applied to optimize the aerodynamic efficiency starting from a simple "dummy" baseline geometry. The aim is to validate the ability of the SBO strategy to globally explore the design space within reasonable timeframe (due to the replacement of the time-consuming CFD tool by the SVM surrogate) while maintaining the accuracy of the results (since the proposed optimal of each iteration is validated with CFD).

Authors have previously validated the accuracy of the SVM-based surrogate model showing mean squared error values between 0.05 and 0.20, which are considered acceptable for this application field. The reader can consult the literature[29,31] for more details about the surrogate model validation. In addition, authors also addressed the problem of designing with high number of design variables starting from configurations that are close to the optimal ones (for instance, airfoils or wings where only small deformations are expected). In this paper, for completeness purposes, the authors aim to validate the feasibility of the approach for optimizing where no clear knowledge about the starting point is provided (this is why the proposed starting point is a clean cylinder) and therefore large deformations are expected in order to reach the optimum.

Table 1. Problem formulation (the Re reference length considered is the cylinder diameter).

M	Re
0.05	1245.22
0.1	2490.45
0.15	3735.67
0.2	4980.90
0.25	6226.13
0.3	7471.35
0.35	8716.58
0.4	9961.81

Application and numerical results

Test case definition

The approach is applied to the aerodynamic shape optimization of a cylinder parametrized as shown in Geometry parameterization section, with the problem formulation defined in Table 1. The location of the design parameters was previously displayed in Figure 1. A symmetric movement of the upper and lower face control points was imposed. The objective function was to minimize drag while preserving, at least, the 80% of the baseline volume, which was considered the minimum valid volume due to structural requirements. This volume preservation was implemented as a strong penalization of the objective function, which allows exploring the whole design space

even if several geometries will finally be discarded by the optimization algorithm. Furthermore, design variables (DVs) are allowed to move ±60% of their initial value in both directions, horizontal and vertical.

The optimization study was performed for different Mach numbers from 0.05 to 0.4, meaning a Reynolds below 10^5 (Table 1), ensuring laminar boundary layer separation conditions, as can be observed in Figure 3.[41] This problem formulation allows using laminar flow conditions; therefore, reducing the required computational cost (compared with turbulence Reynolds Averaged Navier Stokes (RANS) modeling).

Drag minimization of a 3D cylinder for different flow conditions

In this section, the approach is applied to the drag minimization and results are displayed in Tables 2 and 3. In particular, Table 2 shows the optimization results regarding the whole objective function (which includes consideration of both drag and volume values), where it can be seen that the total reduction of the objective function was between 73% and 77% of its original value. Table 3 shows the drag coefficient values of the original and optimized geometries. It can be observed that the drag was minimized between 92% and 94% of its original value in the baseline geometry (depending on the Mach number considered), while at the same time fulfilling the constraints imposed in the volume.

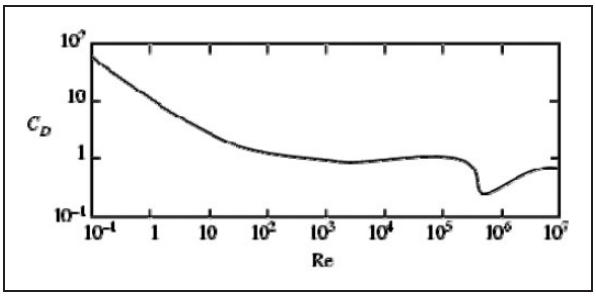

Figure 3. Drag coefficient versus Reynolds number for an infinite circular cylinder (Tritton[41]).

From the abovementioned tables, it can be also observed that the gain in the objective function (OF) relative to the baseline tends to decrease with the Mach number while, on the other hand, the improvement in the drag coefficient tends to increase (see also Figure 4). This behavior is explained because the optimizer proposes thinner shapes as the Mach number increases, producing a geometry with less drag, but also less volume, which is penalized in its global OF.

In addition, Figure 5 shows the evolution of the drag coefficient with the Mach number for the baseline and optimized geometries. In this figure, the line marked with diamonds shows the behavior of the baseline geometry for different Mach numbers and it can be observed how it reproduces well the linear behavior displayed in Figure 3 for Reynolds numbers between 10^3 and 10^4, which correspond to the Mach numbers range considered in this study, as indicated in Table 1. Moreover, the line marked with squares shows the behavior of the drag coefficient in case of the optimized geometries for each of the Mach numbers considered. It can be seen how the drag reduction increases with the Mach number, except for Mach number 0.4, which indicates that the transition region is close.

The optimized shapes returned by the optimizer are displayed in Figure 6. For clarity, only the baseline geometry and the optimized geometries for Mach numbers 0.10, 0.20, 0.30 and 0.40 are shown. It can be observed that all the optimized shapes are similar except the one returned for Mach = 0.40, where the

Table 2. Optimization results.

M	0.05	0.1	0.15	0.2	0.25	0.3	0.35	0.4
$OF_{baseline}$	0.39248	0.30123	0.26356	0.24341	0.23173	0.22510	0.22124	0.21910
OF_{optim}	0.08918	0.07525	0.06751	0.06385	0.06031	0.05784	0.05740	0.05817
%Improvement	77.28	75.02	74.39	73.77	73.97	74.31	74.05	73.45

OF: objective function.

Table 3. Optimization results (C-drag minimization).

M	0.05	0.1	0.15	0.2	0.25	0.3	0.35	0.4
$C\text{-}drag_{baseline}$	0.95672	0.84988	0.80707	0.78708	0.77838	0.77638	0.77909	0.78578
$C\text{-}drag_{optim}$	0.06924	0.05842	0.05241	0.04957	0.04682	0.04490	0.04472	0.04570
$C\text{-}drag_{optim\_p}$	0.05391	0.04875	0.04507	0.04353	0.04162	0.04033	0.04057	0.04189
$C\text{-}drag_{optim\_v}$	0.01532	0.00967	0.00733	0.00604	0.00520	0.00457	0.00415	0.00381
%Improvement	92.76	93.13	93.51	93.70	93.98	94.22	94.26	94.18

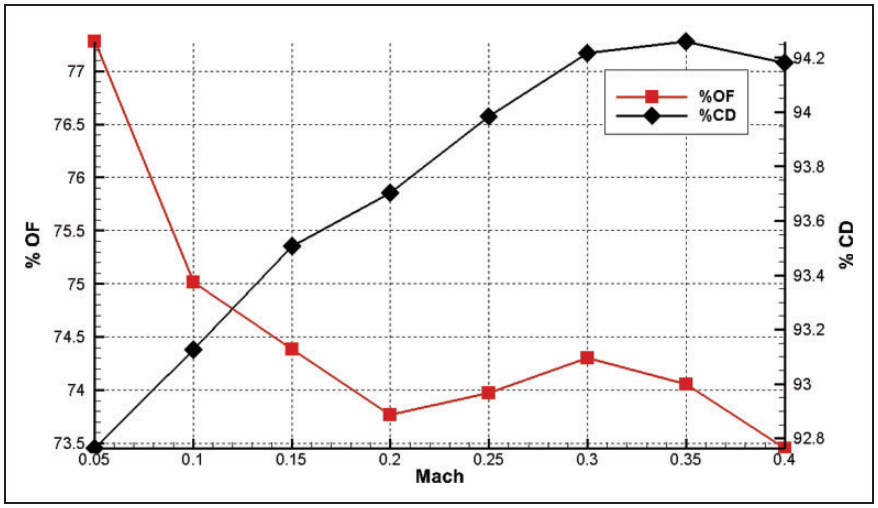

Figure 4. Percentage of improvement on the objective function and on the drag coefficient of the optimized geometries for each of the Mach numbers considered.

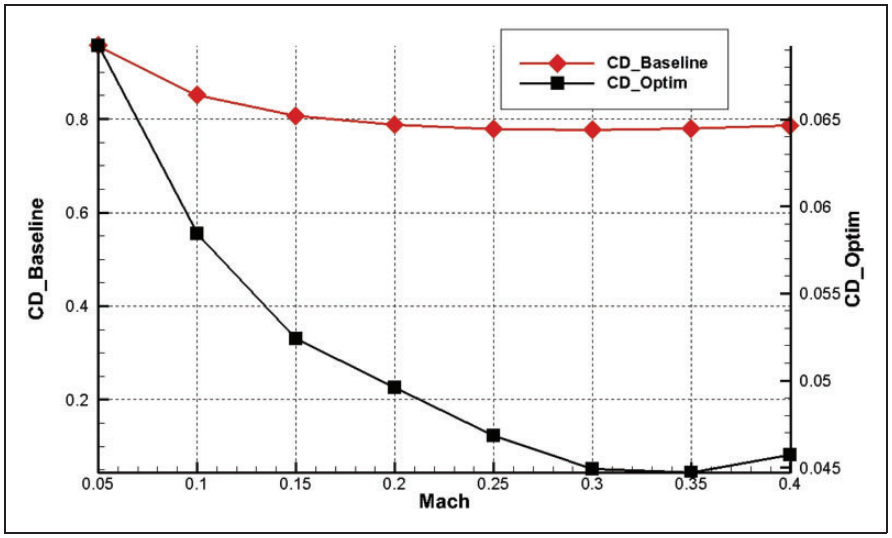

Figure 5. Evolution of the drag coefficients in the baseline and optimized geometries for the Mach numbers considered.

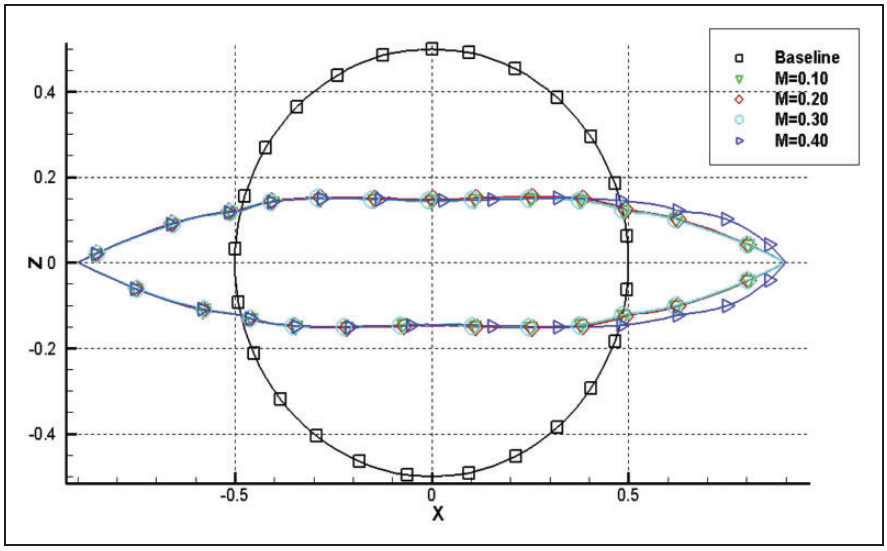

Figure 6. Comparison of baseline and optimal shapes for Mach numbers 0.10, 0.20, 0.30 and 0.40.

optimizer returns a geometry with a wider area near the trailing edge, in order to ensure the volume constraint, even when it will affect the drag value.

The design parameters considered and their allowable movements are schematized in Figure 7. Notice that the control point CP6 is moved symmetrically to CP1 (only in x direction) and control points from CP7 to CP10 are moved symmetrically to control points CP2–CP5 (only in z direction). That means, the movement is in equal magnitude but in opposite direction. In addition, the final values of the design parameters for each of the optimized geometries are displayed in Table 4 (the X and Z values for CP6–CP10 are not included in this table for the reason explained before).

The computational grid used for this optimization study had 100 superficial points and 7k points in total. A total limit of 100 CFD simulations was established for each flow condition. In Figure 8, the convergence of the algorithm is shown (again, for clarity, only the convergence for Mach numbers 0.10, 0.20, 0.30 and 0.40 is shown). It can be seen that the selected limit of 100 CFD runs is more than enough since the optimal is reached around iteration number 20 for all flow conditions. The population of the EA for each iteration was 250 individuals. The total time, including both training, optimization and simulation time (for all the 100 iterations), was about 5 h using one processor on a Linux x86_64 machine.

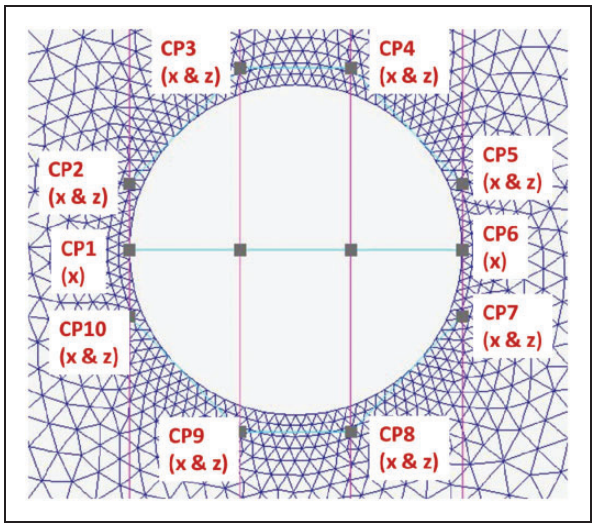

Figure 7. Control points considered in the parameterization and their allowable movements during the optimization.

More interesting, the behavior of the proposed optimization approach (combining SVM, CFD runs and the EA) is displayed in Figure 9. This figure shows the comparison of the OF values predicted by the SVM and computed with the CFD tool for each of the geometries returned in each of the optimization iterations. Also note that the proposed approach returns one geometry per optimization iteration, and that this geometry is always validated with the CFD tool and then used to enrich the surrogate as the optimization evolves. Therefore, the figure includes 100 points (corresponding to each of the 100 geometries from the 100 optimization iterations).

This figure provides two important conclusions:

- First, the use of the SVM-based surrogate does not affect the accuracy of the optimized geometries, since at the end of each iteration, the geometry proposed by the EA is validated with the CFD tool; therefore, the final optimized geometry will be the same as if there were not any surrogate involved in the process. In addition, since the surrogate model is enriched in each of the iterations, in the region close to the optima (see the zoom), the accuracy of the predictions is very high (points are near the line representing exact prediction).
- Second, the proposed approach explores the design space following an optimization-based strategy, which means that the interest is not to produce a surrogate model able to accurately predict the whole design space, but only the region where the optima are located. Therefore, the infill criteria for the surrogate is directly provided by the global optimizer and the new samples are heavily concentrated in a certain region of the design space, as can be also observed in the figure. It is important to notice that the first five points (represented by

Table 4. Geometric variables (X and Z coordinate values) of each control point for the baseline and optimized geometries.

	X1	X2	Z2	X3	Z3	X4	Z4	X5	Z5
Baseline	0.50	0.50	0.20	0.16	0.55	−0.16	0.55	−0.50	0.20
Opt_M0.05	0.89	0.62	0.13	0.20	0.06	−0.20	0.06	−0.60	0.13
Opt_M0.10	0.89	0.60	0.13	0.18	0.06	−0.18	0.06	−0.60	0.13
Opt_M0.15	0.89	0.61	0.13	0.17	0.06	−0.18	0.06	−0.60	0.13
Opt_M0.20	0.89	0.61	0.13	0.18	0.07	−0.18	0.06	−0.60	0.13
Opt_M0.25	0.89	0.89	0.13	0.17	0.06	−0.18	0.06	−0.60	0.13
Opt_M0.30	0.89	0.60	0.13	0.17	0.06	−0.20	0.06	−0.60	0.13
Opt_M0.35	0.89	0.67	0.13	0.18	0.06	−0.19	0.06	−0.60	0.13
Opt_M0.40	0.89	0.78	0.13	0.20	0.06	−0.18	0.06	−0.60	0.13

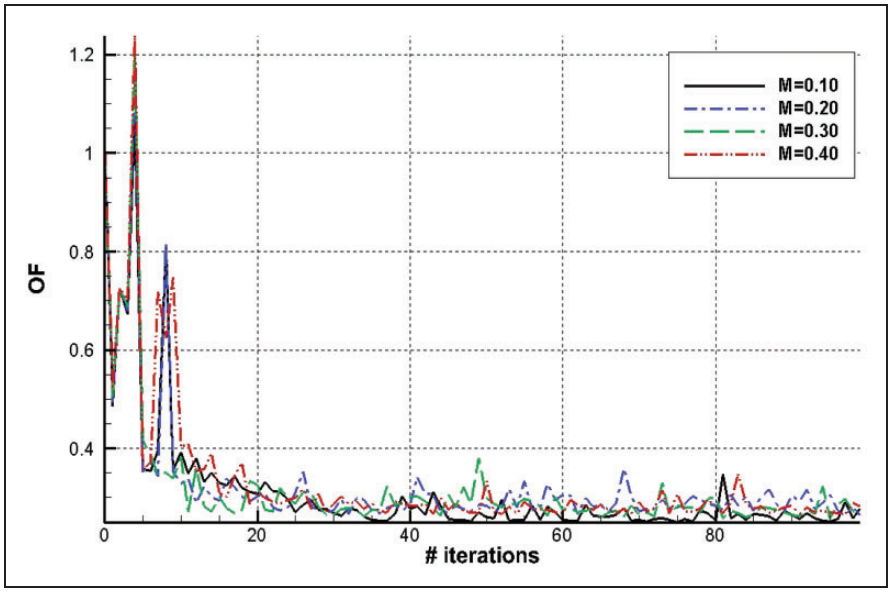

Figure 8. Objective function convergence history.

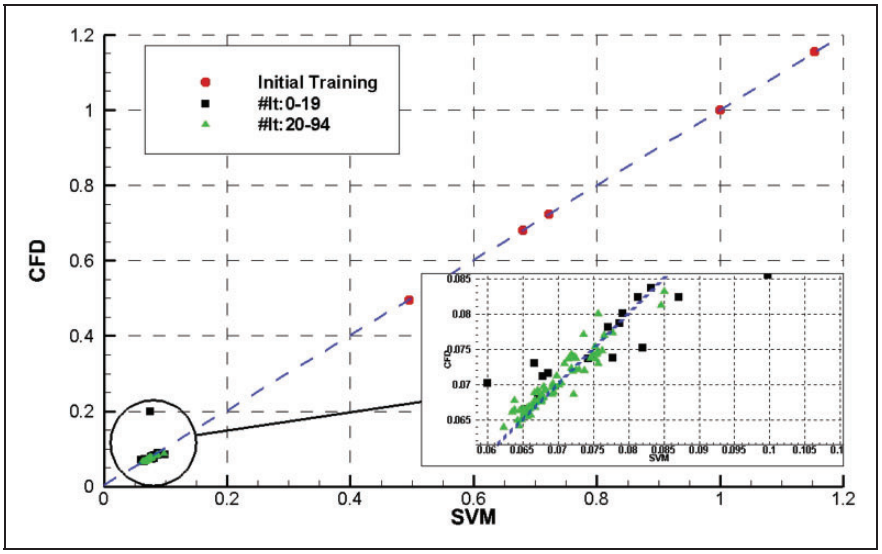

Figure 9. OF values (computed with CFD and SVM) for each of the geometries returned in each of the optimization iterations (a total of 100 geometries are plotted, since 100 optimization iterations were executed).
This plot corresponds to the optimization case for Mach = 0.20 but the behavior for the other optimization is similar.

circles) correspond to the baseline geometry and the four samples generated randomly (as was explained in SBO strategy section) in order to build the first surrogate. Then, the rest of the points displayed are divided in two sets: the squares represent the samples produced by the first 20 iterations of the optimization algorithm (where an acceptable level of convergence is already reached) and the triangles represent the geometries returned in the rest of the iterations. As expected, this approach tends to concentrate more samples in a certain region of the design space (close to the optima) with the evolution of the optimization iterations.

Finally, Figure 10 shows the Mach number contours of the original (left) and optimized (right) geometries for each of the Mach numbers considered in the range [0.05, 0.4]. As expected, a pair of vortices (bigger with the Mach number) appears downstream of the baseline geometry. In the optimized shapes, the cross-sectional area has been reduced as much as the geometric and volume constraints allows. This explains the vortices disappearance and the drag reduction, as expected from the aerodynamic point of view. Some small asymmetric effects can be seen in the Mach contours of the optimized geometries, which are due to volume grid deformation since the geometric surface deformation has to be propagated

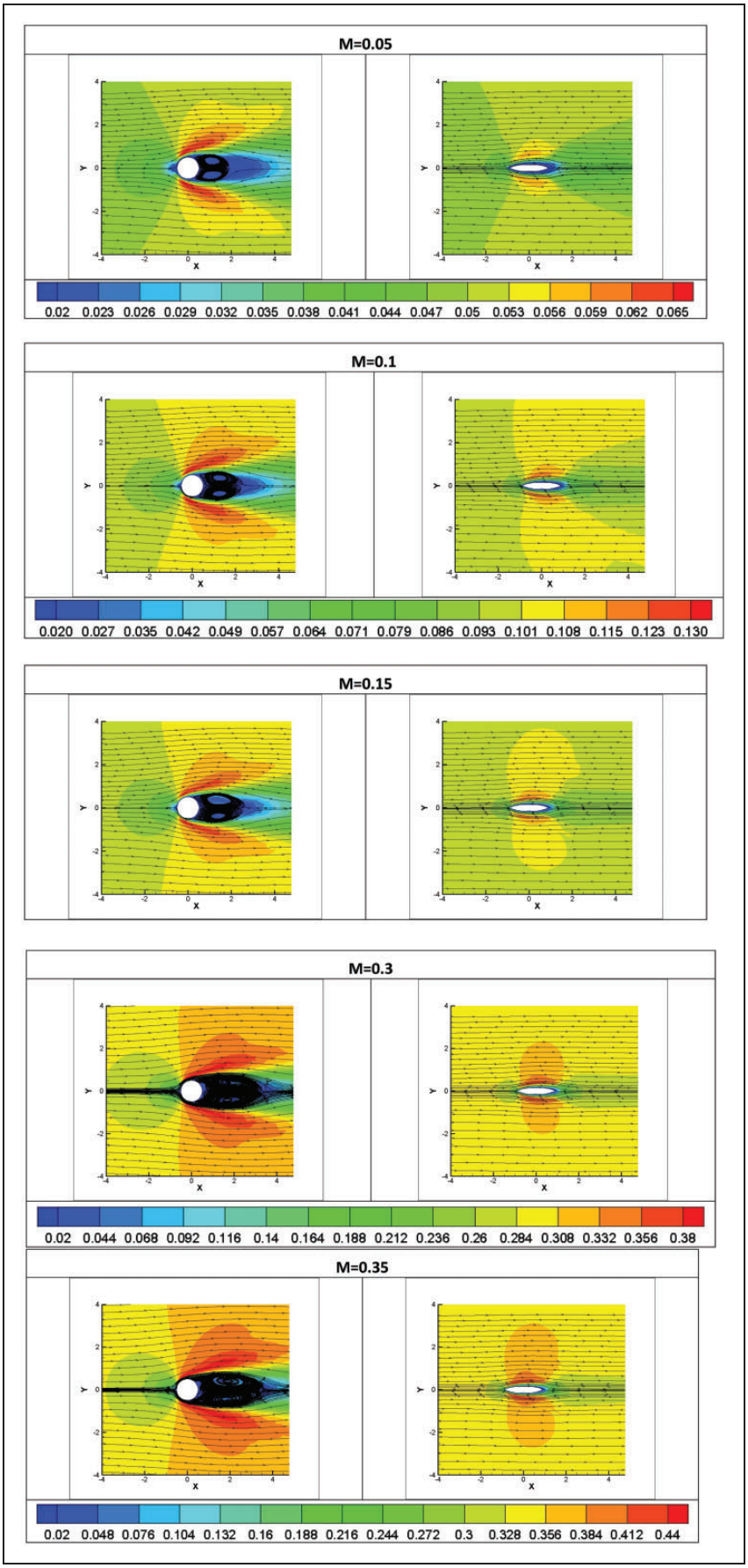

Figure 10. Mach contours and velocity streamlines of the baseline and optimized geometries for different Mach numbers from 0.05 to 0.4.

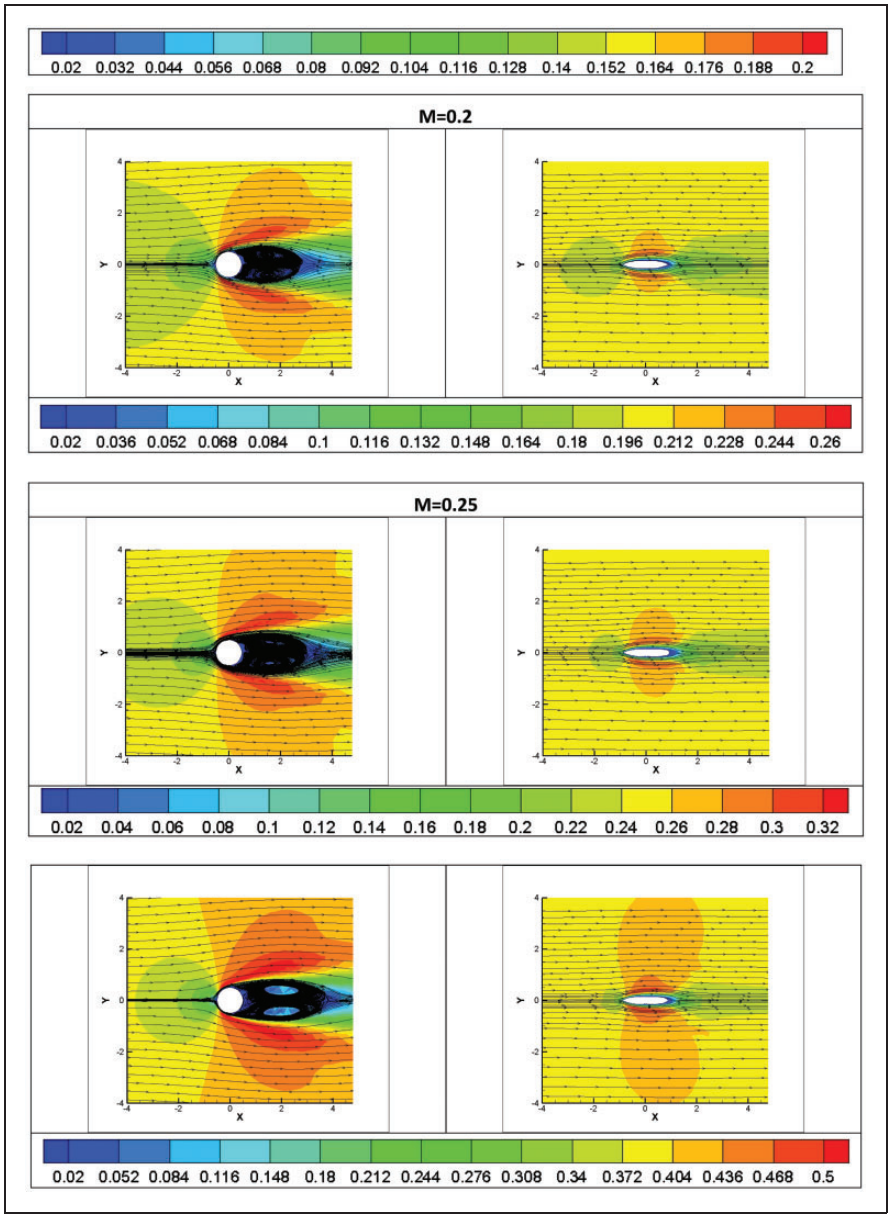

Figure 10. Continued.

to the volume. However, its effect in the accuracy of the solutions is negligible since the quality of the grid elements was checked and showed adequate values.

Conclusions and future research activities

This article presented the application of a global optimization strategy using the IES-SL and the hybridization of EA and SVMs to the aerodynamic shape optimization of a clean cylinder representing a simple model of the landing gear master cylinder. The aim of this work was to demonstrate the feasibility of the proposed technique to reach optimal configurations that are far from the baseline geometry.

The applied approach is able to broadly explore the design space without being dependent on the initial solution. In addition, the approach avoids an extensive use of expensive CFD computations, since it makes use of a metamodel, based on SVMs, to provide an estimate of the aerodynamic coefficients. Finally, with this approach, the accuracy is ensured, since in each iteration, the result is computed with the high fidelity CFD tool.

The obtained results demonstrated that the approach is able to behave well in the drag minimization of the selected test case, providing optimal configurations in an affordable time framework. However, one of the main detected problems when applying this optimization is the mesh deformation, since certain large displacements are produced, which could lead to negative mesh elements. Remeshing may be an option in case of the mentioned large displacements, although its associated computational cost,

and in some cases the need of human interaction, does not make it the desirable option within an automatic optimization framework for complex configurations. Authors' research will focus on this issue and future work will be also dedicated to exploit the results in industry, for the selected test case (landing gear master cylinder), considering further constraints and also including structural aspects that have to be taken into consideration. Another possibility is to use a thickness constraint equal to the diameter of the baseline cylinder for the central control points. In this way, the resulting optimal shape could be used as a "landing-gear fairing", with the underlying cylindrical structure unchanged. This will be also analyzed in future work in order to exploit the industrial applicability of the obtained results.

Declaration of Conflicting Interests

The author(s) declared no potential conflicts of interest with respect to the research, authorship, and/or publication of this article.

Funding

The author(s) received no financial support for the research, authorship, and/or publication of this article.

References

1. ACARE Advisory Council for Aeronautics Research in Europe. Aeronautics and air transport: beyond vision 2020 (towards 2050). Report, ACARE, Publications Office of the European Union, Luxembourg, 2011.
2. Argüelles P, et al. European aeronautics: a vision for 2020. Report, ACARE, Publications Office of the European Union, Luxembourg, 2011.
3. Jameson A, et al. Aerodynamic shape optimization techniques based on control theory. In: *AIAA fluid dynamics conference*, Albuquerque, USA, 15–18 June 1998, AIAA Paper 98-2538.
4. Martin MJ, et al. Non-uniform rational B-splines-based aerodynamic shape design optimization with the DLR TAU code. *J Aerosp* 2012; 226: 1225–1242.
5. Castro C, et al. A systematic continuous adjoint approach to viscous aerodynamic design on unstructured grids. *AIAA Journal* 2007; 45: 2125–2139.
6. Reuther JJ, et al. Constrained multipoint aerodynamic shape optimization using an adjoint formulation and parallel computers, Part 1. *J Aircraft* 1999; 36: 51–60.
7. Lyu Z, et al. Automatic differentiation adjoint of the Reynolds-averaged Navier–Stokes equations with a turbulence model. In: *43rd AIAA fluid dynamics conference and exhibit*, San Diego, California, USA, 24–27 June 2013, AIAA2013-2581.
8. Dwight RP and Brezillon J. Efficient and robust algorithms for solution of the adjoint compressible Navier–Stokes equations with applications. *Int J Numer Methods Fluids* 2009; 60: 365–389.
9. Morris AM, Allen CB and Rendall TCS. Aerodynamic shape optimization of a modern transport wing using only planform variations. *J Aerosp Eng* 2009; 223: 843–851.
10. Brezillon J and Dwight RP. Applications of a discrete viscous adjoint method for aerodynamic shape optimization of 3D configurations. *CEAS Aeronaut J* 2012; 3: 25–34.
11. Lian Y, Oyama A and Liou MS. Progress in design optimization using evolutionary algorithms for aerodynamic problems. *Prog Aerosp Sci* 2010; 46: 199–223.
12. Jin Y, Olhofer M and Sendhoff B. A framework for evolutionary optimization with approximate fitness functions. *IEEE Trans Evol Comput* 2002; 6: 481–494.
13. Jin Y. A comprehensive survey of fitness approximation in evolutionary computation. *Soft Comput J* 2005; 9: 3–12.
14. Santos M, De Mattos B and Girard R. Aerodynamic coefficient prediction of airfoils using neural networks. In: *46th American Institute of Aeronautics and Astronautics, AIAA conference*, Reno, Nevada, 7–10 January, 2008, AIAA2008-887.
15. Asouti VG and Giannakoglou KC. A grid-enabled asynchronous metamodel-assisted EA for aerodynamic optimization. *Genet Program Evolvable Mach* 2009; 10: 373–389.
16. Smoczek J and Szpytko J. Evolutionary algorithm-based design of a fuzzy TBF predictive model and TSK fuzzy anti-sway crane control system. *Eng Appl Artif Intell* 2014; 28: 190–200.
17. KyoungK-jae KK. Financial time series forecasting using support vector machines. *Neurocomputing* 2003; 55: 307–319.
18. Salcedo-Sanz S, et al. Accurate short-term wind speed prediction by exploiting diversity in input data using banks of artificial neural networks. *Neurocomputing* 2009; 72: 1336–1341.
19. Smola A, Schölkopf B and Müller KR. The connection between regularization operators and support vector kernels. *Neural Networks* 1998; 11: 637–649.
20. Zarnani A, et al. Learning to predict ice accretion on electric power lines. *Eng Appl Artif Intell* 2012; 25: 609–617.
21. Li W and Yu J. Predicting contact characteristics for helical gear using support vector machine. *Neurocomputing* 2016; 174: 1156–1161.
22. Leifsson L, Koziel S and Tesfahunegn Y. Aerodynamic design optimization: physics-based surrogate approaches for airfoil and wing design. In: *AIAA SciTech,* Maryland, USA, 13–17 January 2014, AIAA 2014-0572.
23. Li C, Brezillon J and Görtz S. A framework for surrogate-based aerodynamic optimization. In: *ODAS ONERA-DLR aero-space symposium*, Toulouse, France, 9–11 Feb 2011.
24. Koziel S and Leifsson L. Multi-level surrogate-based airfoil shape optimization. In: *51st AIAA aerospace sciences meeting including the new horizons forum and aerospace exposition*, Grapevine (Dallas/Ft. Worth Region), Texas, 7–10 January 2013, AIAA2013-0778.
25. Lukaczyk T, Palacios F and Alonso JJ. Active subspaces for shape optimization. In: *AIAA SciTech*, Maryland, USA, January 2014, AIAA-2014-1171.
26. Iuliano E and Quagliarella D. Aerodynamic Shape Optimization via non-intrusive POD-based surrogate modelling. In: *IEEE congress on evolutionary computation*, Cancún, México, 20–23 June 2013.
27. Jahangirian A and Shahrokhi A. Aerodynamic shape optimization using efficient evolutionary algorithms

and unstructured CFD solver. *Comput Fluids* 2011; 46: 270–276.
28. Ma Y, et al. Hypersonic lifting body aerodynamic shape optimization based on the multiobjective evolutionary algorithm based on decomposition. *J Aerosp* 2015; 229: 1246–1266.
29. Andrés E, et al. Efficient aerodynamic design through evolutionary programming and support vector regression algorithms. *Expert Syst Appl* 2012; 39: 10700–10708.
30. Andrés E, Carro-Calvo L and Salcedo-Sanz S. Fast aerodynamic coefficients prediction using SVMs for global shape optimization. In: *ECCOMAS European congress on computational methods in applied sciences and engineering*, Barcelona, Spain, 20–25 June 2014.
31. Andrés E and Iuliano E. *Application of surrogate-based global optimization to aerodynamic design*. Switzerland: Springer Tracts in Mechanical Engineering, 2015.
32. Chauhan D, Chandrashekarappa P and Duvigneau R. Wing shape optimization using FFD and twist parameterization. In: *12th Aerospace Society of India CFD Symposium*, Bangalore, India, 11–12 Aug 2010.
33. Martin MJ, et al. Volumetric B-splines shape parameterization for aerodynamic shape. *Aerosp Sci Technol* 2014; 37: 26–36.
34. Eiben A and Smith JE. *Introduction to evolutionary computing*. Natural Computing Series. 1st ed. Heidelberg, Berlin: Springer-Verlag, 2003.
35. Ortiz-García EG, et al. Improving the training time of support vector regression algorithms through novel hyper-parameters search space reductions. *Neurocomputing* 2009; 72: 3683–3691.
36. DLR Institute of Aerodynamics and Flow Technology. Technical Documentation of the DLR TAU-Code, 2014.
37. Gerhold T, et al. Calculation of complex three-dimensional configurations employing the DLR TAU-Code. In: *35th aerospace sciences meeting and exhibit,* Reno, NV, USA, 6–9 January 1997, AIAA-97-0167.
38. Forrester AIJ and Keane AJ. Recent advances in surrogate-based optimization. *Prog Aerosp Sci* 2009; 45: 50–79.
39. Koziel S, Echeverría-Ciaurri D and Leifsson L. Surrogate-based methods. In: S Koziel and XS Yang (eds) *Computational optimization, methods and algorithms*. Series: Studies in Computational Intelligence. Heidelberg, Berlin: Springer-Verlag, 2011, pp.33–60.
40. Bandler JW, et al. Space mapping: the state of the art. *IEEE Trans Microwave Theory Tech* 2004; 52: 337–361.
41. Tritton DJ. *Physical fluid dynamic*. 2nd ed. Oxford, UK: Oxford University Press, 1988.